THE JOURNAL OF BIOLOGICAL CHEMISTRY VOL. 289, NO. 2, pp. 909–920, January 10, 2014

The Conserved Lys-95 Charged Residue Cluster Is Critical for the Homodimerization and Enzyme Activity of Human Ribonucleotide Reductase Small Subunit M2*

Received for publication, October 4, 2013, and in revised form, November 18, 2013 Published, JBC Papers in Press, November 19, 2013, DOI 10.1074/jbc.M113.524546

Xinhuan Chen (陈新焕)[‡1], Zhijian Xu (徐志建)[§1], Lingna Zhang (张玲娜)[‡1,2], Hongchuan Liu (刘洪川)[§], Xia Liu (刘霞)[‡], Meng Lou (楼梦)[‡], Lijun Zhu (朱丽君)[‡], Bingding Huang (黄炳顶)[¶], Cai-Guang Yang (杨财广)[§], Weiliang Zhu (朱维良)[§3], and Jimin Shao (邵吉民)[‡4]

From the [‡]Department of Pathology and Pathophysiology, Zhejiang University School of Medicine, Hangzhou 310058, China, the [§]Shanghai Institute of Materia Medica, Chinese Academy of Sciences, Shanghai 201203, China, and the [¶]Genomics and Proteomics Core Facility, German Cancer Research Center, Heidelberg 69120, Germany

Background: Human ribonucleotide reductase small subunit M2 exists in a homodimer form.
Results: Charge-altering mutations of the interfacial residue Lys-95 in M2 prevent its dimer assembly, which inhibits the enzyme activity by interfering with the large subunit M1 binding and subcellular distribution.
Conclusion: The conserved Lys-95 charged residue cluster mediates M2 homodimerization.
Significance: The homodimer form of M2 is indispensable to constitute an active holoenzyme.

Ribonucleotide reductase (RR) catalyzes the reduction of ribonucleotides to deoxyribonucleotides for DNA synthesis. Human RR small subunit M2 exists in a homodimer form. However, the importance of the dimer form to the enzyme and the related mechanism remain unclear. In this study, we tried to identify the interfacial residues that may mediate the assembly of M2 homodimer by computational alanine scanning based on the x-ray crystal structure. Co-immunoprecipitation, size exclusion chromatography, and RR activity assays showed that the K95E mutation in M2 resulted in dimer disassembly and enzyme activity inhibition. In comparison, the charge-exchanging double mutation of K95E and E98K recovered the dimerization and activity. Structural comparisons suggested that a conserved cluster of charged residues, including Lys-95, Glu-98, Glu-105, and Glu-174, at the interface may function as an ionic lock for M2 homodimer. Although the measurements of the radical and iron contents showed that the monomer (the K95E mutant) was capable of generating the diiron and tyrosyl radical cofactor, co-immunoprecipitation and competitive enzyme inhibition assays indicated that the disassembly of M2 dimer reduced its interaction with the large subunit M1. In addition, the immunofluorescent and fusion protein-fluorescent imaging analyses showed that the dissociation of M2 dimer altered its subcellular localization. Finally, the transfection of the wild-type M2 but not the K95E mutant rescued the G_1/S phase cell cycle arrest and cell growth inhibition caused by the siRNA knockdown of M2. Thus, the conserved Lys-95 charged residue cluster is critical for human RR M2 homodimerization, which is indispensable to constitute an active holoenzyme and function in cells.

Ribonucleotide reductase (RR)[5] is a multisubunit enzyme responsible for the reduction of ribonucleotides to their corresponding deoxyribonucleotides, which are building blocks for DNA replication and repair in all living cells. Therefore, the enzyme is critical for the control of cell proliferation and the maintenance of genome stability. The identified regulatory mechanisms for RR activity in cells mainly include gene transcription, protein degradation, allosteric regulation, and subcellular translocation (1–3). A failure in the control of the levels and/or balances of deoxyribonucleotides leads to genetic abnormalities, cancers, or cell death (4, 5).

Three main classes of RR have been described, based on the metal cofactors for the catalytic activity. The class I enzymes require dinuclear metal clusters for activity: an $Fe^{III}Fe^{III}$-tyrosyl radical ($Y^{\bullet}$) cofactor (class Ia), a $Mn^{III}Mn^{III}$-$Y^{\bullet}$ cofactor (class Ib), and a $Mn^{IV}Fe^{III}$ cofactor (class Ic) (6, 7). Class Ia RRs are found in all types of eukaryotes (including human, mouse, and yeast), a few prokaryotes (including *Escherichia coli*), several viruses, and some bacteriophages. This subclass of enzymes is composed of an R1(α_n)R2(β_n) multisubunit protein complex. The large subunit R1 harbors the active site and allosteric sites (1, 8), and the small subunit R2 houses a diiron-tyrosyl radical cofactor essential for generating the active site cysteinyl radical in R1 via a proton-coupled electron transport chain between the two subunits (3, 9). The C-terminal tail of R2 interacts with R1 to form a holoenzyme (10, 11).

* This work was supported by National Natural Science Foundation of China Grants 81372138, 30873094, and 81090421; 863 National High Technology Research and Development Program of China Grants 2012AA020206 and 2012AA01A305; and Ministry of Education of China Grant J20100041.
[1] These authors contributed equally to this work.
[2] Present address: Dept. of Pathology, Taizhou Hospital, Zhejiang Province 317000, China.
[3] To whom correspondence may be addressed: Shanghai Institute of Materia Medica, Chinese Academy of Sciences, Shanghai 201203, China. Tel.: 86-21-50805020; E-mail: wlzhu@mail.shcnc.ac.cn.
[4] To whom correspondence may be addressed: Dept. of Pathology and Pathophysiology, Zhejiang University School of Medicine, Hangzhou 310058, China. Tel.: 86-571-88208209; E-mail: shaojimin@zju.edu.cn.

[5] The abbreviations used are: RR, ribonucleotide reductase; SASA, solvent-accessible surface area; MM/GBSA, molecular mechanics/generalized Born surface area; MM/PBSA, molecular mechanics/Poisson-Boltzmann surface area; MD, molecular dynamics; PDB, Protein Data Bank; TRITC, tetramethylrhodamine isothiocyanate; EYFP, enhanced yellow fluorescent protein.

There exist different oligomeric states of class Ia RRs, and a common active form has been proposed to be a transient $(\alpha_2)_a(\beta_2)_b$ complex (3, 12), which is allosterically regulated by the nucleoside triphosphates (13). Under physiological conditions, *E. coli* RR exists as a mixture of transient $\alpha_2\beta_2$ and $\alpha_4\beta_4$ species whose distributions are modulated by allosteric effectors (12, 14). The yeast *Saccharomyces cerevisiae* RR comprises α and $\beta\beta'$ subunits in an $(\alpha_2)_a(\beta\beta')_b$ active holoenzyme (15–17). Mammalian genomes contain a single R1 gene (also named as M1 in human RR) and two R2 genes for R2 and its homologue p53R2 (also named as M2 and M2B, respectively, in human RR). For eukaryotic RRs, the ATP/dATP-induced R1 multimers can interact with R2 dimers to form active $\alpha_2\beta_2$, $\alpha_6\beta_2$, or $\alpha_6\beta_6$ complexes or inhibited $\alpha_6\beta_2$ complexes (8, 18–20).

It seems that the dimer form of R1 and R2 is a basic entity in an active RR holoenzyme. R1, monomeric in the absence of ligands, dimerizes in the presence of substrate or effectors (21). When the allosteric substrate specificity effectors bind to one R1 monomer, a minor conformational change is induced in a connecting loop that influences binding of the correct substrate to the second R1 monomer. Therefore, R1 dimer formation is a prerequisite to function properly (18, 22). R2 forms a homodimer in cells (23, 24). However, using heterodimers containing deuterated tyrosine on the full-length side and protonated tyrosine on the truncated side, Sjöberg *et al.* (25) found that the tyrosyl radical is randomly generated in either of the two polypeptide chains of the heterodimeric R2 subunit in *E. coli*. In a recent study on *S. cerevisiae* RR, Zhang *et al.* (17) demonstrated that the C-terminal tails of $\beta\beta'$ interact only with the proximal α within each α/β (α/β') pair in the holoenzyme. Although each monomer of R2 from *E. coli*, mouse, or human possesses a diiron-tyrosyl radical site and a set of residues for the radical transfer to M1, one monomer probably can function independently for the radical generation and R1 binding to form an active complex. In this case, however, the contribution of the dimer form of the small subunit to the function of a class Ia RR holoenzyme is a fundamental biological question.

In this study, we identified a conserved cluster of charged residues, including Lys-95, Glu-98, Glu-105, and Glu-174, at the homodimer interface in human RR small subunit M2 based on its x-ray crystal structure in combination with site mutagenesis and functional analysis. We demonstrated that the conserved Lys-95 charged residue cluster is critical for M2 homodimer assembly, which is indispensable to constitute an active holoenzyme and function in cells.

EXPERIMENTAL PROCEDURES

Prediction of Dimer Interface Residues Based on M2 Structure—The M2 crystal structure was retrieved from the protein data bank (PDB code 3OLJ) (Fig. 1*A*). First, solvent-accessible surface areas (SASAs) for each residue of the dimer were calculated. Second, the dimer was split into two pieces, one for each protomer. Third, the protomer-only SASA for each residue was calculated. Last, the difference between the dimer-based SASA and the protomer-only-based SASA was calculated for each residue. If the value was greater than 0.75 $Å^2$, it was defined as an interface residue (Fig. 1*B*). The calculations were performed with a PyMOL script.

Computational Alanine Scanning—Alanine, glycine, and proline are not suitable for computational alanine scanning. Except for these residues, each interface residue predicted above was mutated to alanine (26). The binding free energies (ΔG_{bind}) of the wild-type and alanine mutants were calculated using the molecular mechanics/generalized Born surface area (MM/GBSA) (27) approach and molecular mechanics/Poisson-Boltzmann surface area (MM/PBSA) (28) approach, which are programmed in the AMBER9 package. The energy difference between the mutant and the wild-type M2 ($\Delta\Delta G_{mut-WT}$) was calculated as $\Delta\Delta G_{mut-WT} = \Delta G_{mut} - \Delta G_{WT}$. $\Delta\Delta G_{mut-WT}$ is a measure of the contribution of the interface residues to M2 dimerization. A larger absolute value indicates a higher contribution.

To carry out computational alanine scanning, a molecular dynamics (MD) simulation was performed to obtain a set of equilibrium conformations of the dimer. MD simulations were carried out for M2 dimer structure using the AMBER9 package (29) with the ff03 AMBER force field (30). After removing alternative conformations, the protonation states of histidine were assigned manually. The M2 dimer was solvated by a rectangular box of TIP3P (31) waters extended at least 10.0 Å in each direction from the dimer. Then sodium ions were added to generate a neutral simulation system. 2000 steps of minimization were performed in order to minimize the system with the protein restrained, Cα restrained, and the whole system relaxed. The system was heated up in two steps using a Langevin temperature equilibration scheme with restraints on the protein. First, with the backbone restrained, a constant volume periodic boundary was used to heat the system from 0 to 300 K in 20 ps. Second, with Cα restrained, a constant pressure periodic boundary was used to equilibrate the system at 300 K over a time scale of 100 ps. Finally, a 20-ns MD equilibration was run on the whole system with constant pressure at 300 K. The Langevin dynamics was used to control the temperature at 300 K with a collision frequency of 2.0 ps^{-1}. A pressure-coupling algorithm was used to maintain the pressure with a relaxation time of 2 ps. The SHAKE algorithm (32) was used to constrain bonds involving hydrogen, which allowed for a 2-fs time step during the heating and equilibration phases, and the particle-mesh Ewald algorithm (33, 34) was used to calculate long distance electrostatic interactions with a cut-off of 10.0 Å.

It was found that the system was equilibrated after 10 ns (Fig. 1*C*). A total of 200 snapshots were saved during the equilibration stage for computational alanine-scanning analysis, one snapshot per 50 ps of dynamic simulation. The binding free energy differences ($\Delta\Delta G_{mut-WT}$) between the mutants and the wild-type M2 ($\Delta G_{mut} - \Delta G_{WT}$) from MM/GBSA calculations are shown in Fig. 1*D*, whereas the detailed data are presented in Table 1. A positive $\Delta\Delta G_{mut-WT}$ value implies a positive contribution to the M2 dimerization.

Plasmid Construction—pET28a-M2 and pET28b-M1 constructs for the full-length small and large subunit proteins of human RR were prepared previously (35). The coding sequence of M2 was inserted into pcDNA3.1 vector with a FLAG tag at the N terminus, a 2× HA tag at the C terminus, or a 6× Myc tag at the C terminus and also inserted into pEYFP vector with an EYFP tag at the C terminus. The coding sequence of M1 was

TABLE 1

Changes of MM/GBSA and MM/PBSA binding free energies (kcal/mol) caused by the alanine mutations at the interface of M2 homodimer

M2	$\Delta G_{bind,\ GB}$ [a]	$\Delta\Delta G_{mut-WT,\ GB}$	$\Delta G_{bind,\ PB}$ [b]	$\Delta\Delta G_{mut-WT,\ PB}$
R79A	−28	27	−14	37
E147A	−35	20	−28	23
R159A	−42	13	−4	47
K95A	−42	13	−37	15
F83A	−44	11	−43	8
F80A	−45	11	−47	5
R78A	−48	7	−41	11
F101A	−49	6	−49	3
Y94A	−50	6	−57	−5
I82A	−50	5	−52	0
F194A	−50	5	−48	4
W91A	−51	4	−53	−2
F164A	−52	4	−51	1
V81A	−52	3	−48	4
N170A	−53	3	−50	2
Q151A	−53	2	−49	2
I166A	−53	2	−48	3
I171A	−53	2	−54	−3
T103A	−54	2	−48	4
I197A	−54	1	−50	1
S150A	−54	1	−52	0
N195A	−55	1	−51	1
C160A	−55	0	−53	−1
L178A	−55	0	−52	0
WT	−55	0	−52	0
E174A	−56	0	−58	−6
N142A	−56	−1	−52	−1
S173A	−56	−1	−52	0
E143A	−56	−1	−53	−2
S177A	−56	−1	−53	−2
E198A	−57	−1	−52	0
V146A	−57	−2	−51	1
E191A	−58	−3	−54	−2
D181A	−58	−3	−55	−4
E105A	−60	−5	−59	−7
E98A	−63	−7	−67	−16

[a] GB, MM/GBSA.
[b] PB, PB/GBSA.

inserted into pcDNA3.1 vector with a 6× Myc tag at the N terminus. The mutants were generated using the QuikChange™ site-directed mutagenesis kit (Stratagene, La Jolla, CA) according to the manufacturer's instructions. The primers for the above constructs are listed in Tables 2 and 3. All constructs were verified by DNA sequencing.

Cell Culture and Transfection—HEK 293T and HeLa cells were cultured in Dulbecco's modified Eagle's medium (Invitrogen), and KB cells were cultured in RPMI 1640 (Invitrogen), both supplemented with 10% fetal bovine serum (Invitrogen). Transient plasmid transfections were performed with X-tremeGENE HP DNA Transfection Reagent (Roche Applied Science), and siRNA transfections were performed with Lipofectamine RNAiMAX Reagent (Invitrogen) per the manufacturer's recommendations.

Preparation of Recombinant Proteins—The recombinant M1 and M2 proteins were expressed from BL21 (DE3) bacteria with the pET28a-M1 and pET28b-M2 constructs and were purified using nickel-nitrilotriacetic acid-agarose resin (Qiagen, Valencia, CA) affinity chromatography according to the Qiagen protocol (36). Protein concentration was measured with the Bio-Rad protein assay kit, and protein purity was determined by SDS-PAGE. The proteins were placed in aliquots and frozen at −70 °C.

Size Exclusion Chromatography—The recombinant proteins were diluted to a concentration of 600 μg/ml. Gel filtration was performed with a buffer composed of 50 mM Tris-HCl (pH 7.5), 150 mM NaCl, and 2 mM dithiothreitol (DTT) at 4 °C, using the AKTA fast protein liquid chromatography system equipped with a Superdex 200 10/300 column (GE Healthcare). The

TABLE 2

Primers used for construction of M2 and M1 protein expression plasmids

Plasmid	Primer	Sequence
pcDNA3.1-HA-M2(WT)	F(XhoI)	5′-ACG**CTCGAG**CTACCATGCTCTCCCTCCGTGTC-3′
	R(BamHI)	5′-ATCC**GGATCC**GAAGTCAGCATCCAAGGTA-3′
pcDNA3.1-c-Myc-M2(WT)/FLAG-M2(WT)	F(BamHI)	5′-ATCC**GGATCC**ACCATGCTCTCCCTCCGTGTC-3′
	R(XhoI)	5′-ACG**CTCGAG**GAAGTCAGCATCCAAGGTA-3′
pcDNA3.1-c-Myc-M1(WT)	F(NotI)	5′-AAT**GCGGCCGC**ATGCATGTGATCAAGC-3′
	R(XbaI)	5′-CG**TCTAGA**TCAGGATCCACACATCAGACATT-3′
pEYFP-M2(WT)	F(XhoI)	5′-ACG**CTCGAG**CTACCATGCTCTCCCTCCGTGTC-3′
	R(BamHI)	5′-C**GGATCC**GTGAAGTCAGCATCCAAG-3′

TABLE 3

Primers used for construction of M2 mutant proteins

Boldface letters denote the mutated codons.

Mutant	Primer sequence (forward)
R78A	AGAGAAAACCCC**GCC**CGCTTTGTCATCTTCCCC
R78E	GCTGCTGAGAGAAAACCCC**GAA**CGCTTTGTCATCTTCCC
R79A	GAGAAAACCCCCGC**GCC**TTTGTCATCTTCCCC
F80A	AGAGAAAACCCCCGCCGC**GCT**GTCATCTTCC
F83A	CCGCTTTGTCATC**GCC**CCCATCGAGTACCATG
K95A	GGCAGATGTAT**GCG**AAGGCAGAGGCTTCCTTTTGG
K95E	CTGGCAGATGTAT**GAG**AAGGCAGAGGCTTCC
K95Q	CTGGCAGATGTAT**CAG**AAGGCAGAGGCTTCC
E98A	GTATAAGAAGGCA**GCG**GCTTCCTTTTGGACCG
E98K	GTATAAGAAGGCA**AAG**GCTTCCTTTTGGACCGCC
E98A/K95E	GTAT**GAG**AAGGCA**GCG**GCTTCCTTTTGGACCG
E98K/K95E	GTAT**GAG**AAGGCA**AAG**GCTTCCTTTTGGACCGCC
F101A	GTATAAGAAGGCAGAGGCTTCC**GCT**TGGACCGCC
E105A	CCTTTTGGACCGCC**GCG**GAGGTTGACCT
E147A	GGCATAGTAAATGAAAACTTGGTG**GCG**CGATTTAGCC
E147R	GCAAGCGATGGCATAGTAAATGAAAACTTGGTG**AGA**CGATTTAGCC
R159A	CCAAGAAGTTCAGATTACAGAAGC**CGC**CTGTTTCTATGGC
E174A	GCCATGGAAAACATACATTCT**GCA**ATGTATAGTCTTCTTATTGAC
E191A	CCAAAGAAAGG**GCA**TTTCTCTTCAATGCCATTGAAACG
R264Q	ACTTATTAGC**CAA**GATGAGGGTTTACACTGTGATTTTGCTTGCC
M2(no-tag)-3′	GATGCTGACTTC**TGA**TCCTACCCATACGATGTTC

molecular weight and oligomeric state of the proteins were estimated based on the standard curve generated by a Bio-Rad molecular mass marker kit, which included thyroglobin (670 kDa), γ-globulin (158 kDa), ovalbumin (44 kDa), myoglobulin (17 kDa), and vitamin B_{12} (1.35 kDa).

Co-immunoprecipitation and Immunoblotting Analysis—For interaction between HA-M2 and c-Myc-M2, the cell lysates were prepared at 48 h after transfection using radioimmune precipitation assay buffer containing 50 mM Tris-HCl (pH 7.4), 1% Nonidet P-40, 0.25% (w/v) sodium deoxycholate, 150 mM NaCl, 1 mM phenylmethanesulfonyl fluoride (PMSF), 10 g/ml leupeptin, 10 g/ml aprotinin, 1 mM vanadate, and 1 mM NaF. The lysates were clarified by centrifugation at 13,000 × *g* for 15 min at 4 °C. The supernatant was quantified and incubated overnight at 4 °C with 4 μl of anti-mouse c-Myc (Santa Cruz Biotechnology, Inc.). The mixture was then incubated with 20 μl of 50% protein G Plus-agarose (Santa Cruz Biotechnology, Inc.) for 4 h at 4 °C with gentle rocking. After three washes in radioimmune precipitation assay buffer, the immunoprecipitates were separated on SDS-PAGE (10%), transferred to nitrocellulose membrane, and blocked with TBS containing 5% (w/v) skim milk and 0.1% Tween 20. Primary antibodies included rabbit anti-human HA, or rabbit anti-human c-Myc (both from Santa Cruz Biotechnology, Inc.). Membranes were incubated with the primary antibody overnight at 4 °C, washed three times with TBS containing 0.1% Tween 20, and then stained with Alex 680- or IR 800- conjugated secondary antibody (LI-COR, Lincoln, NE) for LI-COR analysis.

For interaction between FLAG-M2 and c-Myc-M1, the cell lysis buffer was as follows: 1× phosphate-buffered saline (PBS), 1% Nonidet P-40, 0.5% (w/v) sodium deoxycholate, 0.1% (w/v) SDS, 1 mM PMSF, 10 g/ml leupeptin, 10 g/ml aprotinin, 1 mM vanadate, and 1 mM NaF (37). Proteins were immunoprecipitated with rabbit anti-human c-Myc antibody and detected by immunoblotting using rabbit anti-human FLAG antibody (Santa Cruz Biotechnology, Inc.).

RR Activity Assay and Competitive Inhibition—The CDP reduction activity of the recombinant RR proteins was assayed according to our previous procedure (35, 38). The reaction mixture contained 0.125 μM [^{3}H]CDP, 50 mM Hepes (pH 7.2), 100 mM KCl, 6 mM DTT, 4 mM magnesium acetate, 2 mM ATP, 0.05 mM CDP, and mixed recombinant proteins of M2 and M1 at a 1:1 ratio (each 0.5–1 μM) in a final volume of 100 μl. After incubation at 37 °C for 15–30 min and dephosphorylation, samples were analyzed by HPLC and liquid scintillation counting. For competitive inhibition of the enzyme activity, the M2 mutant protein (R264Q or K95E) was serially diluted in 25 mM Tris-HCl (pH 7.4) and incubated with the wild-type M2 and M1 proteins at room temperature for 30 min. Then the RR activity was analyzed as described above.

Cellular RR activity assays were performed as described previously (39). Briefly, cultured cells were lysed in a low salt homogenization buffer (10 mM Hepes, pH 7.2, and 2 mM DTT) by 20 passages through a 27-gauge needle on ice. Then the same volume of high salt buffer (1 M Hepes, pH 7.2, 2 mM DTT) with protease inhibitors was added and passed through the needle again. The supernatants were collected after centrifugation, and proteins were eluted by gel size exclusion (Sephadex G-25, GE Healthcare). The protein concentration and the RR activity in the cellular extracts were determined as above. RR activity = dCDP/(CDP + dCDP) × 100%.

Electron Paramagnetic Resonance (EPR) Measurements—The wild-type and mutant M2 proteins were regenerated as described previously (38, 40, 41). Briefly, a solution containing 1.5 mM ferrous iron ($FeCl_2$) and 200 mM DTT was added to the fresh purified R2 protein solutions in 50 mM Tris-HCl (pH 7.4) and 0.1 M KCl to give a final concentration of 10 mM DTT and 75 μM ferrous iron. Then air was bubbled through the solution, and the mixture was incubated for 15 min at 25 °C. The protein was passed through gel filtration on a Sephadex G25 column. After incubation at room temperature for different intervals, the protein samples were frozen in liquid nitrogen, and the X-band EPR spectra were measured with a Bruker EMX spectrometer equipped with an Oxford helium cryostat. The instrumental parameters were as follows: T = 30 K; microwave frequency, 9.376 GHz; microwave power, 0.5 milliwatt; modulation amplitude, 4 Gauss; and modulation frequency, 100 kHz (35, 38). Radical concentrations were determined by a comparison with a standard sample of 1 mM Cu^{2+}, 10 mM EDTA.

Inductively Coupled Plasma Optical Emission Spectrometry—The iron content of the regenerated wild-type and mutant M2 proteins was measured using a PerkinElmer Life Sciences inductively coupled plasma optical emission spectrometer (Optima 8000DV, PerkinElmer Life Sciences) after acid digestion of the samples. Pure iron standard solution (Shanghai Institute of Measurement and Testing Technology) was serially diluted from 10 to 1000 mg/liter to construct the standard curve ($y = 183{,}770x$; x, concentration; y, absorbance; $R^2 = 1$).

Indirect Immunofluorescence Microscopy—The cells were fixed in 4% (w/v) paraformaldehyde and permeabilized with 0.2% Triton X-100. Then the samples were blocked with 1% (w/v) bovine serum albumin, stained in sequence with mouse anti-FLAG antibody (Sigma), TRITC-conjugated secondary antibody, and DAPI (42). The cells were visualized using a confocal microscope (Zeiss LSM 510 META).

Imaging of EYFP Fusion Proteins—HeLa cells were transiently transfected with either the wild-type or a mutant M2 construct carrying EYFP marker. Cells were imaged 48 h after transfection using a Nikon Eclipse Ti-S microscope.

Cell Cycle Analysis—HeLa cells were harvested, fixed in cold 70% ethanol, and stained with propidium iodide solution after transfection with the human RR M2 gene-specific siRNA (Santa Cruz Biotechnology, Inc.) and plasmid constructs encoding the wild-type or K95E mutant M2 for 48 h. The scramble siRNA (Santa Cruz Biotechnology, Inc.) and empty vector were used as controls. The cell cycle was analyzed by flow cytometry, and the data were analyzed using the WinMDI program.

Cell Proliferation Assays—HeLa cells were plated in 96-well plates at 2 × 10^4 cells/well. After transfection for 72 h, cell viabilities were assayed using a cell-counting kit (CCK-8, Dojindo (Kumamoto, Japan)).

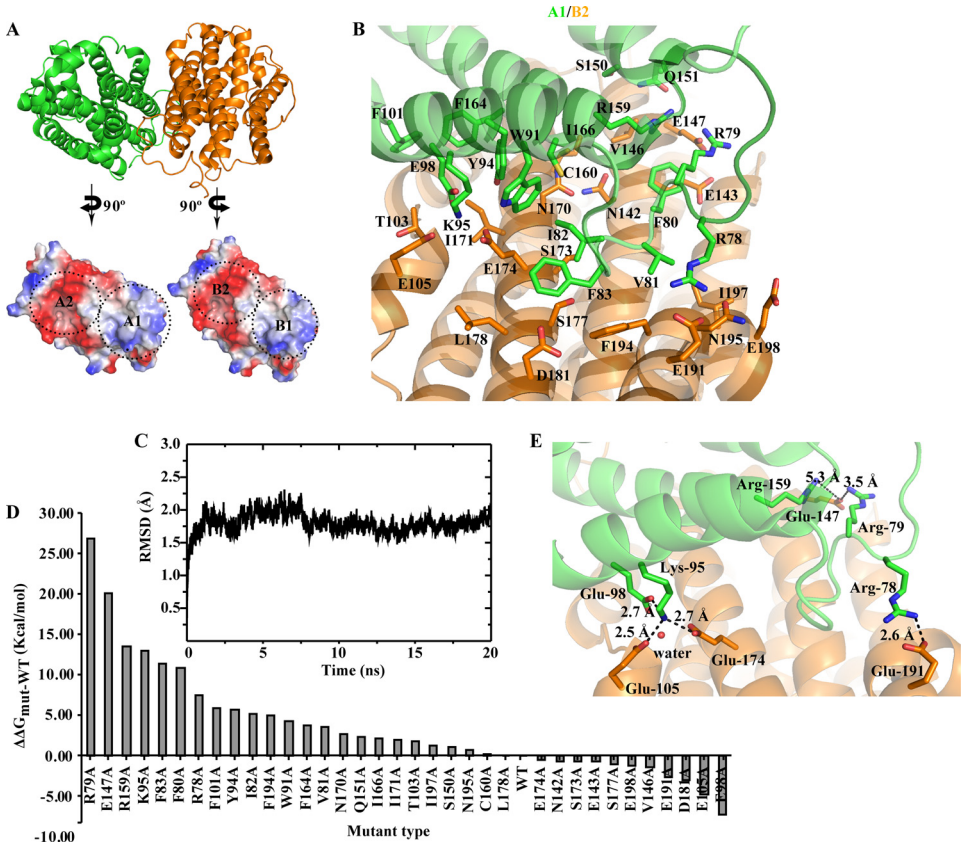

FIGURE 1. *A*, *top*, the crystal structure of human ribonucleotide reductase M2 homodimer (PDB code 3OLJ), in which the protomer 1 and 2 are *colored green* and *orange*, respectively. *Bottom*, an "open book" view of the interaction interface between the two protomers. The interaction sites are divided into two patches in each protomer (*i.e.* A1 and A2 in one protomer and B1 and B2 in the other protomer). A1 is identical to B1, and A2 is identical to B2. The interaction mode between the two protomers is A1-B2 and A2-B1. The positive charge potential and negative charge potential are depicted in *blue* and *red*, respectively. *B*, the residues on the A1-B2 interface are shown in *sticks*; the identical A2-B1 interface is omitted for clear visualization. *C*, root mean square deviation (*RMSD*) of M2 dimer during the MD simulation with respect to its starting structure. *D*, computational alanine scanning of the interface residues. Binding free energy differences ($\Delta\Delta G_{mut-WT}$) between the mutant M2s and the wild-type M2 ($\Delta G_{mut} - \Delta G_{WT}$) were from MM/GBSA calculations. *E*, based on the computational alanine scanning prediction, three clusters of charged residues on the M2 homodimer interface might mediate the dimer assembly. The distances between the salt bridge pairs are shown in angstroms. A water molecule in close contact to the Lys-95 cluster is shown as a *sphere*.

RESULTS

Identification of the Amino Acid Residues That Mediate M2 Dimerization—Human RR small subunit M2 is a homodimer, and the dimer interface can be divided into two identical interaction sites (*i.e.* A1 interacts with B2 and A2 interacts with B1, where A1 is identical to B1 and A2 is identical to B2 based on the M2 crystal structure (PDB code 3OLJ)) (Fig. 1*A*). Based on the SASA difference between the dimer and protomer, 42 residues were identified at the interface of the M2 dimer: Pro-77, Arg-78, Arg-79, Phe-80, Val-81, Ile-82, Phe-83, Pro-84, Trp-91, Tyr-94, Lys-95, Glu-98, Phe-101, Thr-103, Glu-105, Ala-135, Ala-136, Gly-139, Asn-142, Glu-143, Val-146, Glu-147, Ser-150, Gln-151, Arg-159, Cys-160, Gly-163, Phe-164, Ile-166, Ala-167, Asn-170, Ile-171, Ser-173, Glu-174, Ser-177, Leu-178, Asp-181, Glu-191, Phe-194, Asn-195, Ile-197, and Glu-198 (Fig. 1*B*). After removing alanine, glycine, and proline, which are not suitable for computational alanine scanning, 35 residues were left and used to estimate the binding free energy changes as a result of mutating the interfacial residues to alanine. To carry out computational alanine scanning, a MD simulation was preformed to obtain a set of equilibrium conformations of the dimer. It was found that the system was equilibrated after 10 ns (Fig. 1*C*). The computational alanine scanning by MM/GBSA suggested that Arg-79, Glu-147, Arg-159, Lys-95, Phe-83, Phe-80, and Arg-78 contribute significantly to M2 dimerization (Fig. 1*D* and Table 1). Similar results were also obtained from MM/PBSA calculations (Table 1). Combined analysis with the crystal structure of M2 dimer suggested that three clusters of interfacial charged residues might be responsible for the dimerization (Fig. 1*E*) (*i.e.* Arg-78^1/Glu-191^2 or Arg-78^2/Glu-191^1, Arg-79^1/Glu-147^2/Arg-159^1 or Arg-79^2/Glu-147^1/Arg-159^2, and Lys-95^1/Glu-98^1/Glu-105^2/Glu-174^2 or Lys-95^2/Glu-98^2/Glu-105^1/Glu-174^1 (the residues in protomer 1 or protomer 2 are distinguished by superscript number 1 or 2, respectively)). In addition, several hydrophobic residues at the interface of the M2 dimer, such as Phe-80, Phe-83, and Phe-101, might also contribute to dimer formation.

The K95E Mutation Prevents M2 Dimerization and Inhibits RR Activity—To test whether the above identified residues are responsible for M2 dimerization, a series of expression plasmids for the wild-type and mutant M2 proteins were constructed. The charge-opposite mutants for the three clusters of interfacial charged residues included R78E, K95E, and E147R. The alanine mutants included R78A, R79A, F80A, K95A, E147A, R159A, E174A, E191A, and E98A. After co-transfecting HA-M2 and c-Myc-M2 into HEK 293T cells, co-immunopre-

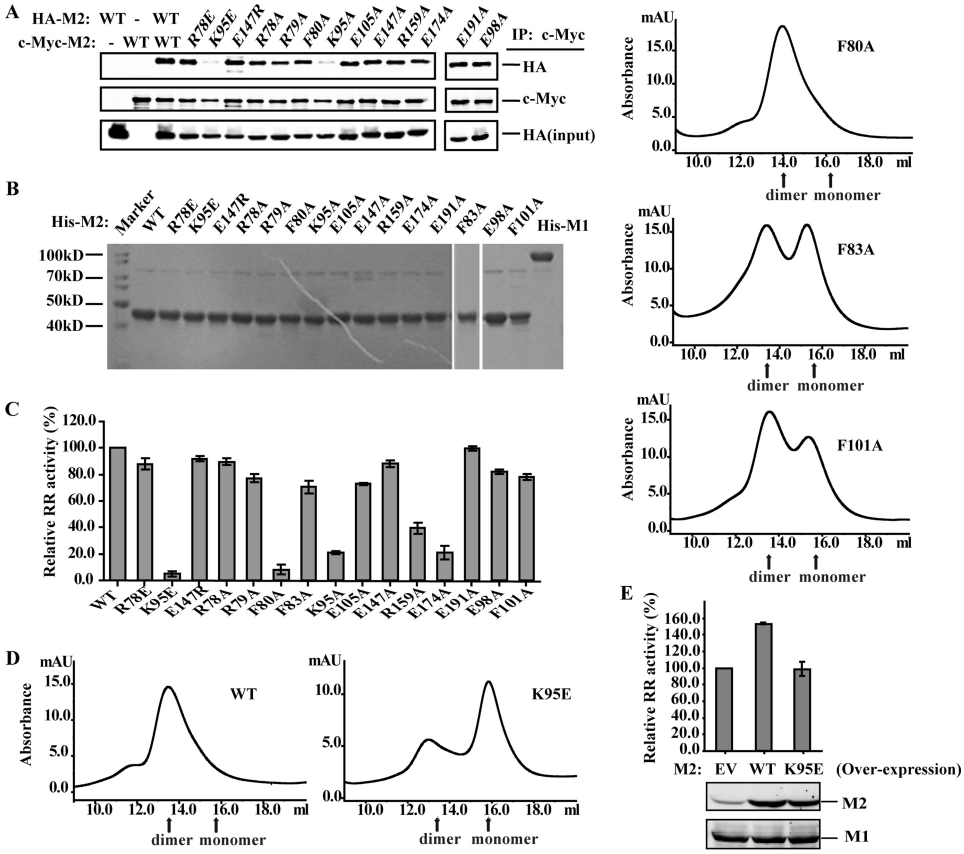

FIGURE 2. *A*, HEK 293T cells were co-transfected with the expression plasmids for the wild-type and mutant M2 proteins with a HA or c-Myc tag as indicated. The cell lysates were prepared at 48 h after transfection, and the co-immunoprecipitations (*IP*) were performed with anti-c-Myc antibody followed by immunoblotting detection with anti-HA antibody. Ten percent of the cell lysate for each co-immunoprecipitation was used for the input control. *B*, SDS-PAGE (10%) analysis of the purity and homogeneity of the His-tagged recombinant M2 and M1 proteins purified by nickel resin affinity chromatography. *C*, the recombinant M2 and M1 proteins were mixed and assayed for the CDP reduction activity, as described under "Experimental Procedures." The enzyme activity of each mutant M2 protein is presented as a percentage of that for the wild type. *D*, size exclusion chromatography measurements were conducted for the recombinant wild-type and mutant M2 proteins. The protein elution using 50 mM Tris-HCl (pH 7.5), 150 mM NaCl, and 2 mM DTT was monitored by absorbance at 280 nm with a set of molecular mass markers. *E*, KB cells were transfected with empty vector (*EV*) and the wild-type and K95E mutated M2 plasmids, respectively. The expressions of the M2 proteins in KB cells were shown using immunoblotting examination. The relative RR activity in the cellular lysates was measured as above. *Error bars*, S.D.

cipitation experiments showed that the interaction between either the two K95E mutants or the two K95A mutants was reduced significantly compared with that between the wild-type or other mutant M2 proteins (Fig. 2*A*). The RR activity assays with the recombinant M2 and M1 proteins (Fig. 2*B*) showed that the K95E mutation in M2 sharply attenuated the enzyme activity to 4.9 ± 2.1% compared with the wild-type protein (Fig. 2*C*). The size exclusion chromatography experiments using the recombinant M2 proteins showed that the wild-type M2 ran as a dimer, whereas the K95E mutant was mainly in a monomer form (Fig. 2*D*). Furthermore, the overexpression of wild-type M2 in KB cells markedly increased the intracellular RR activity, but the K95E mutant failed (Fig. 2*E*).

The possible role of hydrophobic interactions in the dimer assembly was also examined. The RR activity and M2 dimer formation were affected by the F83A and F101A mutations but much less than by the K95E/A mutation (Fig. 2, *C* and *D*). The F80A mutation significantly inhibited the enzyme activity (Fig. 2*C*); however, both the co-immunoprecipitation and size exclusion chromatography experiments indicated little interference in the dimer formation by the mutation (Fig. 2, *A* and *D*). The above results suggested that Lys-95 plays an important role in M2 dimerization, and the Lys-95[1]/Glu-98[1]/Glu-105[2]/Glu-174[2] cluster (hereafter referred to as the Lys-95 charged residue cluster) is probably a key interfacial site for the dimer assembly. In addition, the hydrophobic residues at the interface may also aid the dimer formation.

The Charge-exchanging Co-mutation of K95E and E98K Recovers M2 Dimerization as Well as RR Activity—In the Lys-95 charged residue cluster, only Lys-95 is a positively charged residue. The double mutations of K95E and E98K for charge-exchanging between the two residues were introduced into the Lys-95 charged residue cluster. After transfecting into HEK 293T cells, co-immunoprecipitation experiments showed that the K95E/E98K double mutant, which exchanged the charge property between Lys-95 and Glu-98, restored the interaction between the two monomers compared with the K95E single mutation (Fig. 3*A*). The K95Q mutant, which introduced a glutamine into the Lys-95 charged residue cluster, interfered less with the dimerization than the K95E mutant.

Size exclusion chromatography and RR activity assays were performed using the recombinant RR proteins (Fig. 3*B*). The gel filtration examinations showed that the K95E/E98K double mutations and the K95Q mutation fully and partially recovered

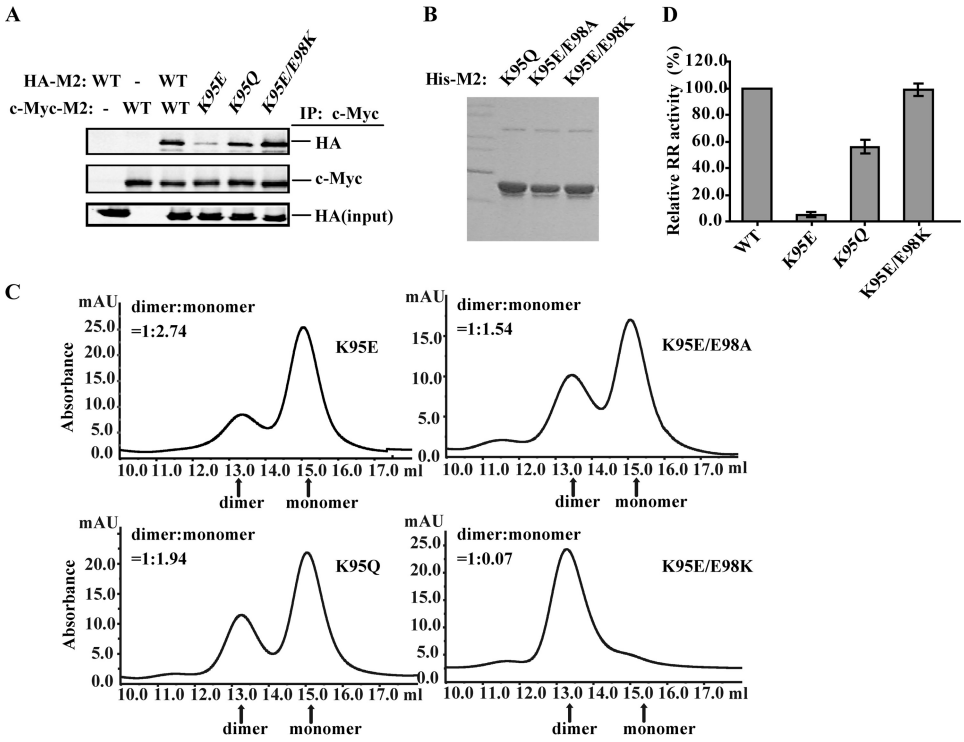

FIGURE 3. *A*, the wild-type and mutant HA-M2 and c-Myc-M2 constructs were co-transfected into HEK 293T cells. The cell lysates were then co-immunoprecipitated using anti-c-Myc antibody and were examined by immunoblotting using anti-HA antibody. Ten percent of each cell lysate for the co-immunoprecipitation was used for the input control. *B*, SDS-PAGE (10%) analysis of the purity and homogeneity of the His-tagged recombinant M2 proteins purified by nickel resin affinity chromatography. *C*, size exclusion chromatography was performed with the recombinant wild-type and mutant M2 proteins as indicated. *D*, the RR activity of the recombinant M2 proteins was measured and presented as described above. *Error bars*, S.D.

the dimerization of M2, respectively, compared with the K95E mutation and the K95E/E98A double mutations (Fig. 3*C*). The RR activity assays further confirmed that whereas the K95E mutation almost quenched the enzyme activity, the K95Q mutant and the K95E/E98K double mutant possessed 55.9 ± 5.3 and 99.0 ± 4.9% of the wild-type M2 activity, respectively (Fig. 3*D*). The results suggested that the Lys-95 charged residue cluster couples the two monomers across the interface most likely through an "ionic lock"-like mechanism, where the positively charged Lys-95 plays a key role in balancing the negative charges from the other three glutamic acid residues (Glu-98, Glu-105, and Glu-174).

The Lys-95 Charged Residue Cluster Is Conserved in the Small Subunits of Class Ia RRs—To investigate whether the charge interaction in the Lys-95 cluster site is conserved in class Ia RR small subunits, structural superposition analysis was performed between human M2, human p53R2, mouse R2, *E. coli* R2, yeast RNR2-RNR4 heterodimer, and yeast RNR2-RNR2 homodimer, respectively (Fig. 4). It was shown that the Lys-95 cluster is highly conserved among the small subunits of human, mouse, and yeast RRs. In the eukaryotic RR small subunits, a conserved water is found in the charged residue cluster, which may contribute to the stabilization of the cluster by mediating a hydrogen bond network. Despite the low sequence identity of 20% between human M2 and *E. coli* R2, it seems that the charged residue cluster still exists with Lys-95-M2 substituted by Glu-41-*E. coli* R2 and Glu-174-M2 substituted by Arg-120-*E. coli* R2, respectively; in addition, Glu-37-*E. coli* R2, corresponding to Trp-91-M2, probably plays a role as Glu-98-M2 for the charge balance at the interface. Thus, the "ionic lock" mechanism for the assembly of M2 dimer is probably conserved in class Ia RR small subunits.

The K95E Mutation Does Not Interfere with the Generation of the Diiron and Tyrosyl Radical Cofactor in M2—The diiron and tyrosyl radical cofactor in M2 is essential for RR activity. Structural analysis suggested that the Lys-95 mutations should not affect the diiron site or tyrosyl radical site within the same protomer because the distances are 25.3 and > 15.3 Å between Lys-95 and the radical site Tyr-176 and the iron ligands, respectively (Fig. 5*A*). However, Glu-174, one of the Lys-95 cluster residues, resides on the same α helix as the radical residue Tyr-176 and the iron ligand residue His-172, with only a one-residue interval, raising a possibility that the mutations on Lys-95[2] may affect the essential residues Tyr-176[1] and His-172[1] through interfering with Glu-174[1] (Fig. 5*A*). However, EPR analyses showed that the K95E mutant maintained the tyrosyl radical to a similar extent as wild-type M2 at different time points up to 120 min at room temperature (Fig. 5*B* and Table 4). Inductively coupled plasma optical emission spectrometry measurements showed that the iron content of the wild-type and K95E mutant M2 proteins was similar (Table 4). The results suggested that the M2 monomer (the K95E mutant) was capable of generating and maintaining the diiron and tyrosyl radical cofactor, although it failed to constitute an active RR. This also excluded the possibility that the quenching of the RR activity in the K95E mutant resulted from interfering with the essential cofactor formation and stability.

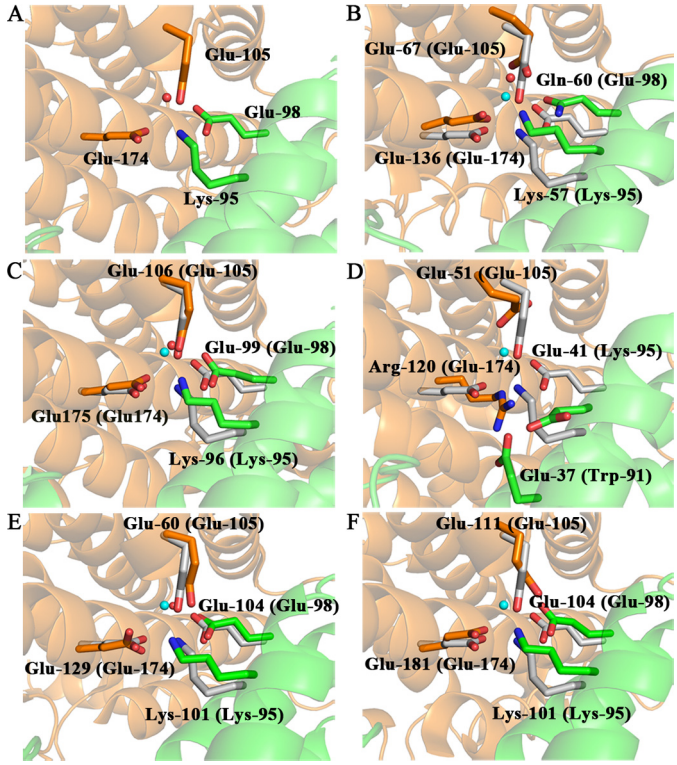

FIGURE 4. **The superimposition of human M2 (PDB code 3OLJ) (*A*) with human p53R2 (PDB code 3HF1) (*B*); mouse R2 (PDB code 1W68) (*C*), *E. coli* R2 (PDB code 1MXR) (*D*), yeast RNR2-RNR4 heterodimer (PDB code 1JK0 (*green* for RNR2, *orange* for RNR4) (*E*), and yeast RNR2-RNR2 homodimer (PDB code 1SMQ) (*F*).** The residues in protomer 1 are *colored green*, whereas the residues in protomer 2 are *colored orange*. Water molecules are shown as *red spheres* in the structures of human M2, human p53R2, mouse R2, and yeast RNR2-RNR4. In *B–F*, the residues corresponding to those in M2 (residue numbers are given in *parentheses*) are shown with *gray sticks*, and water sites corresponding to those in M2 are shown as *cyan spheres*.

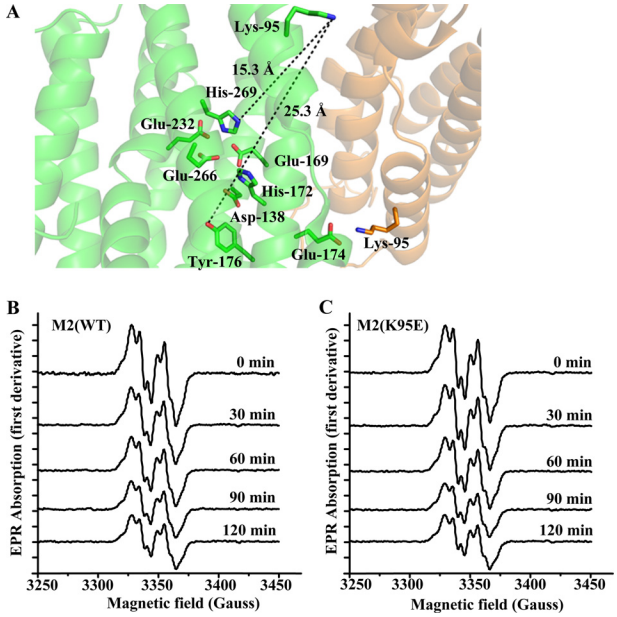

FIGURE 5. *A*, Lys-95 in protomer 2 may affect His-172 and Tyr-176 through interference with Glu-174 in protomer 1 (PDB code 3OLJ). Protomers 1 and 2 are *colored green* and *orange*, respectively. Iron ligand residues (Asp-138, Glu-169, His-172, Glu-232, Glu-266, and His-269), Tyr-176, Glu-174, and Lys-95 are shown in *sticks*. *B*, the tyrosyl radical intensity of the wild-type and K95E mutant M2 proteins was determined by EPR measurements. The freshly purified recombinant M2 proteins were regenerated with $FeCl_3$ and DTT, incubated at room temperature for different times as indicated, and then frozen in liquid nitrogen. The EPR spectra were recorded as described under "Experimental Procedures."

TABLE 4

The radical quantification and iron content of the wild type and mutant M2 proteins

Protein	M2(WT)	M2(K95E)
Radical content (Tyr˙/dimer)		
0 min	0.638	0.662
30 min	0.520	0.553
60 min	0.437	0.428
90 min	0.375	0.375
120 min	0.381	0.374
Iron content (iron/dimer)	3.32 ± 0.009	3.48 ± 0.019

The K95E Mutation in M2 Affects Its Interaction with M1 and Localization in Cells—Co-immunoprecipitation was employed to examine whether the disassociation of M2 dimer by the K95E mutation affects the interaction between the small and large subunits of RR. The result showed that the binding between the K95E mutant M2 and the wild-type M1 was significantly decreased in the co-transfected cells in comparison with the wild-type M2 (Fig. 6*A*). Arg-265-mouse R2 is conserved in all known sequences of the small subunits of class Ia RRs. The R265Q mutation in mouse R2 depleted its RR activity but had minor effects on tyrosyl radical generation and the binding of M2 to M1 (43). The R264Q mutant M2 (corresponding to Arg-265-mouse R2) was used for competitive enzyme inhibition assays (Fig. 6*B*). The result showed that the R264Q-M2 was capable of competing with the wild-type M2 to bind to M1 and hence inhibiting the enzyme activity. In comparison, the K95E mutant exhibited a much lower competitive ability to inhibit the enzyme activity, reflecting that the K95E mutant possessed a significantly reduced ability to bind M1. The results suggested that the disruption of M2 dimer reduced its interaction with M1 to form an active holoenzyme in cells.

Human RR subunits, including M2, are mainly distributed in the cytoplasm under normal growth conditions (44). The nuclear localization of RR subunits is associated with dynamic changes in RR enzymatic activity and nuclear proportions of dNTPs at the G_1/S phase transition (37, 44). Indirect immunofluorescence confocal microscopy (Fig. 6*C*) and EYFP fusion protein-fluorescent imaging (Fig. 6*D*) showed that whereas the wild-type M2 was predominantly located in the cytoplasm, the K95E mutant changed its distribution to both the cytoplasm and nucleus, and the K95E/E98K double mutants reversed the disordered distribution. The results suggested that the dimer form of M2 is important for its normal subcellular distribution.

The K95E Mutant Fails to Rescue the G_1/S Phase Cell Cycle Arrest and Cell Proliferation Inhibition Induced by M2 siRNA Knockdown—During the cell cycle, M2 is only expressed in the late G_1/early S phase for DNA replication. Inhibition of M2 prevents cell cycle progression and cell proliferation. Flow cytometry analysis showed that the transfected expression of the wild-type M2 reversed the G_1/S phase cell cycle arrest induced by the siRNA knockdown of M2, whereas the K95E mutant did not (Fig. 7*A*). Furthermore, cell proliferation assays showed that the transfection of the wild-type M2 but not the K95E mutant rescued the cell growth (Fig. 7*B*). The corre-

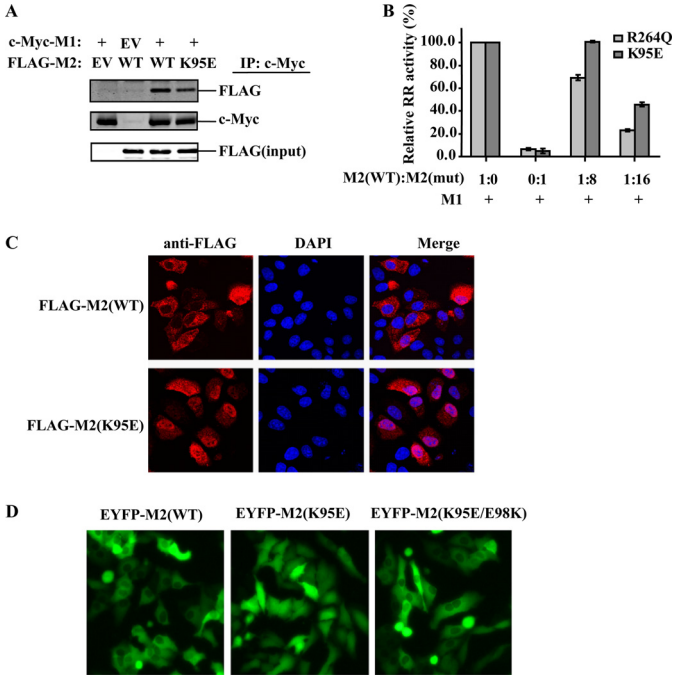

FIGURE 6. *A*, HEK 293T cells were co-transfected with the wild-type or mutant M2 and M1 constructs as indicated. The cell lysates were prepared at 48 h after transfection and then were co-immunoprecipitated with anti-c-Myc antibody and detected by immunoblotting using anti-FLAG antibody. Ten percent of each cell lysate for the co-immunoprecipitation was used for the input control. *B*, competitive enzyme inhibition assays of the wild-type M2 by the K95E or R264Q mutant M2 proteins. The mixing proportions of the wild type (0.4 μM) and mutant M2 proteins were 1:0, 0:1, 1:8, and 1:16, respectively. Each M2 mixture sample was assayed for the RR activity in the presence of the M1 protein (0.4 μM). The enzyme activity of the mutant M2 was presented as a percentage of the wild-type activity. *C*, HeLa cells were transfected with either the wild-type (*flag-M2(WT)*) or mutant (*flag-M2(K95E)*) M2 construct (~45 kDa for monomer). The cells were incubated with mouse anti-FLAG antibody and then TRITC-conjugated (*red*) anti-mouse IgG secondary antibody. Nuclei were counterstained with DAPI (*blue*). Cells were observed under a Zeiss 510 confocal microscope. *D*, HeLa cells were transfected with either the wild-type (*EYFP-M2(WT)*) or mutant (*EYFP-M2(K95E)* or *EYFP-M2(K95E/E98K)*) M2 construct (~70 kDa for monomer). Cells were observed under a Nikon Eclipse Ti-S microscope. *Error bars*, S.D.

sponding M2 expression levels were examined by immunoblotting (Fig. 7*C*).

DISCUSSION

The small subunits of class Ia RRs are dimeric *in vitro* and in cells (45–47). However, it is still unclear how the two protomers interact with each other and whether each protomer can function as an independent unit for RR activity. In this study, structure-based molecular dynamics simulations and alanine scanning analysis suggested that three clusters of charged residues (Arg-78^1/Glu-191^2, Arg-79^1/Glu-147^2/Arg-159^1, and Lys-95^1/Glu-98^1/Glu-105^2/Glu-174^2) at the homodimer interface may mediate the assembly of human RR small subunit M2 (Fig. 1). Site-directed mutagenesis combined with co-immunoprecipitation of the M2 proteins in the transfected cells and size exclusion chromatography analysis using the purified M2 proteins showed that the Lys-95 charged residue cluster (Lys-95^1/Glu-98^1/Glu-105^2/Glu-174^2) played a pivotal role in the dimerization (Fig. 2, *A* and *D*). RR activity assays indicated that the disassembly of M2 dimer by the K95E mutation almost eliminated the enzyme activity *in vitro* and in cells (Fig. 2, *C* and *E*). Whereas the K95Q mutant partially recovered the dimerization and the enzyme activity in comparison with the K95E mutant, the K95E/E98K double mutations that maintain the charge balance at the Lys-95 cluster completely recovered the dimer form and enzyme activity (Fig. 3). The evidence demonstrated that the Lys-95 charged residue cluster functions as critical salt bridges for the dimer assembly, and the dimer form of M2 is essential for human RR activity.

It was suggested based on structural analyses over past 20 years that *E. coli* R2 dimer interaction is formed by the first layer of helices, the first β-pleated sheet strand, and the random-coil structure of the N-terminal residues (45); the subunit interface of mouse R2 is held together mainly by hydrophobic interactions, such as with Phe-102, Phe-165, and Ala-168, and charged interactions may also occur in the dimer interface, such as Lys-96 interacting with Glu-106, Glu-175, and Glu-99, and Arg-160 with Glu-144 and Glu-148 (48); in addition, the interaction of Arg-80 with Glu-144 and also that of Arg-79 with Glu-192 are possibly involved in the interface interaction (49). However, there was no further biological evidence to support these predictions.

The eukaryotic R2s share about 60–82% sequence identity, whereas it is 25% between *E. coli* and mouse R2 (48). Our study demonstrated that among the three clusters of charged residues at the dimer interface of human M2 (Fig. 1*E*), the Lys-95 cluster (Lys-95^1/Glu-98^1/Glu-105^2/Glu-174^2), corresponding to Lys-96/Glu-106/Glu-175/Glu-99 in mouse R2 (50), was well structure-superimposed with the small subunits of other representative class Ia RRs (Fig. 4). The *in vitro* and *in vivo* biological analyses revealed that the charged interaction of in the Lys-95 cluster was critical to M2 dimer formation (Figs. 2 and 3). The conservation suggests a common function of the Lys-95 charged residue cluster in class Ia RR small subunits. We also examined the contribution of the other two clusters (Arg-78^1/Glu-191^2 and Arg-79^1/Glu-147^2/Arg-159^1), which partially correspond to the predicted residues in mouse R2 (49, 50), to the dimerization and activity of M2. However, co-immunoprecipitation and RR activity assays showed a less important role of the two clusters for the dimerization (Fig. 2, *A* and *C*).

Our computational alanine scanning predicted that the interfacial hydrophobic residues, such as Phe-80, Phe-83, and Phe-101 (corresponding to Phe-81, Phe-84, and Phe-102 in mouse R2), might be involved in human M2 dimer assembly (Fig. 1*D*). The size exclusion experiments and RR assays showed that Phe-83 and Phe-101 had a certain influence on M2 dimer formation and enzyme activity (Fig. 2, *C* and *D*). Although the F80A mutation significantly reduced the RR activity, it did not affect the dimerization of M2, as shown in co-immunoprecipitation and size exclusion chromatography experiments (Fig. 2, *A*, *C*, and *D*). Multiple mechanisms are involved in the regulation of RR activity in mammalian cells (51). The critical role and related mechanism of Phe-80 for human M2 activity are worth studying in the future. Thus, all of the experimental evidence suggested that the K95E charged residue cluster plays a comparatively more important role in human M2 dimer formation.

There are two primary possibilities that the dimer form of M2 is essential for the enzyme activity of human RR. The first possibility is that the dissociation of M2 dimer by the K95E

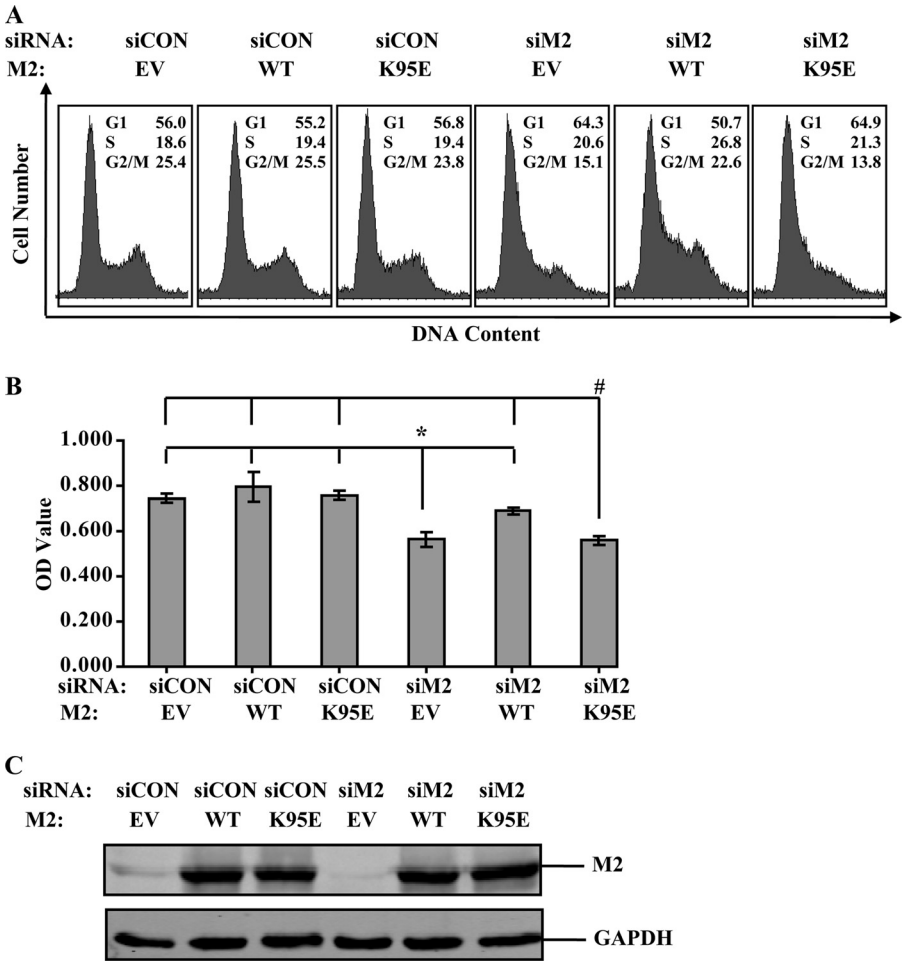

FIGURE 7. **HeLa cells were transfected with the specific siRNA against human RR M2 gene (*siM2*) or the scramble siRNA (*siCON*) as control.** The construct encoding the wide type or K95E mutant M2 protein or the empty vector control (*EV*) was co-transfected with siM2 or siCON, respectively. The cells were harvested for cell cycle analysis by flow cytometry (*A*) and for the cell proliferation assay using the CCK-8 cell-counting kit (in triplicate; * and #, $p < 0.05$, *t* test) (*B*). *C*, the expression of the wild type and mutant M2 proteins in the transfected cells were measured by the immunoblotting method. *Error bars*, S.D.

mutation may affect the generation or stability of the activity-essential diiron-tyrosyl radical cofactor in M2. However, the measurements of the radical and iron contents showed that the K95E mutant housed the diiron and tyrosyl radical cofactor similarly to the wild-type M2 (Fig. 5 and Table 4), indicating that the disruption of the dimer interaction by the K95E mutation has no significant impact on the activity-essential cofactor in M2. The second possibility is that the disassembly of M2 dimer may interfere with its interaction with M1 because the dimer conformation is probably required for M1 binding and the PCET between the two subunits. This hypothesis was supported by the co-immunoprecipitation investigations and competitive enzyme inhibition assays (Fig. 6, *A* and *B*). The above evidence suggested that although the monomer was capable of generating the activity-essential cofactor similar to the dimer, the conformation of the dimer form was needed for M1 binding to constitute a functional human RR. In the future, the structure determination of an active holo-class Ia RR will help to further clarify this mechanism.

The RR small subunit of *S. cerevisiae* is a $\beta\beta'$ heterodimer. β' is structurally homologous to β but lacks important ligating side chains and contains no metallocofactor. Although β' is catalytically inactive, it is required for converting β into a conformation that is competent for iron loading and $Y^{\bullet}$ formation by forming a stable 1:1 $\beta\beta'$ complex *in vitro* and *in vivo* (16, 17, 46). Human RR M2 is a homodimer. We showed that the generation and stability of the diiron-tyrosyl radical cofactor was not dependent on the dimer form; however, a monomer probably lacks the quaternary structure for binding and communicating with M1.

The reduction of ribonucleotides is the rate-limiting step of DNA synthesis. Cell cycle-regulated R2 is responsible for providing dNTPs in actively dividing cells, and the DNA damage-inducible p53R2 is required for replenishing dNTP pools in cells under genotoxic stress (50, 52). Because of its critical function in DNA replication and repair, RR is tightly regulated in cells by multiple mechanisms, including subcellular translocation. There are two opinions about the intracellular location of dNTP synthesis in mammalian cells. In early studies, R1 and R2 were observed to predominantly localize to the cytoplasm. Therefore, ribonucleotide reduction was thought to take place in the cytoplasm, and the dNTPs were presumed to be transported into the nucleus for DNA synthesis (53). Recently, the "replitase" model has suggested that NDPs, rather than free dNTPs, are "channeled" directly into DNA synthesis in the nucleus. It is argued that RR subunits translocate into the

nucleus individually and assemble there to form the active holoenzyme (54). In response to DNA damage, human M2 and p53R2 move rapidly from the cytoplasm into the nucleus to form an active complex to ensure the local availability of dNTPs at DNA damage sites for repair (37). However, the translocation mechanism of mammalian RR subunits in cells is still unclear. In *S. cerevisiae*, three mechanisms are involved in the distribution and translocation of R2: Dif1-dependent nuclear import, retention by the nuclear anchor Wtm1, and Crm1-mediated nuclear export (55, 56). However, no similar anchoring or transporting mechanisms have been reported for R2 in mammalian cells so far. Our immunofluorescent and EYFP fusion protein-fluorescent microscopy analyses showed that whereas the wild-type M2 mainly located in the cytoplasm, the K95E mutant changed its distribution to both the cytoplasm and nucleus (Fig. 6, *B* and *C*). The disordered distribution due to M2 dimer disassembly may disturb the exertion of RR function in cells. It is possible that only the dimer form of M2 possesses an appropriate conformation for passing through the nuclear pore or can interact properly with certain proteins similar to that in *S. cerevisiae* for normal distribution in cells, which deserves further investigation.

RR is a critical enzyme for cell fate. Increased expression and activity of human RR has been associated with malignant transformation and cancer development, which makes it an important target for anticancer agents (57) RR inhibitors, such as the small compounds hydroxyurea, triapine, and gemcitabine; the antisense oligonucleotides, such as GTI-2040; and some oligopeptides inhibiting R1-R2 polymerization have been used in clinical cancer treatment or are being vigorously investigated (58) Our study demonstrated that disruption of M2 dimerization extinguished the enzyme activity of human RR, suggesting that disruption of M2 dimerization is a potential strategy for RR inhibition.

In summary, this study demonstrated for the first time that the conserved Lys-95 charged residue cluster plays a predominant role in M2 dimerization, which is essential for human RR activity *in vitro* and *in vivo*. Disassembly of the M2 dimer affects its interaction with the large subunit and its distribution in cells, ultimately leading to abnormality of the function of human RR. These new findings extend our understanding of the structural architecture and functional mechanism of the multisubunit enzyme RR and may propose a potential site for the design of novel RR inhibitors.

Acknowledgments—We thank Dr. Wei Tong (High Magnetic Field Laboratory, Chinese Academy of Sciences) for the EPR measurements. We thank Dr. Sheng Ye (Life Sciences Institute, Zhejiang University) for insightful comments.

REFERENCES

1. Jordan, A., and Reichard, P. (1998) Ribonucleotide reductases. *Annu. Rev. Biochem.* **67,** 71–98
2. Nordlund, P., and Reichard, P. (2006) Ribonucleotide reductases. *Annu. Rev. Biochem.* **75,** 681–706
3. Hofer, A., Crona, M., Logan, D. T., and Sjöberg, B. M. (2012) DNA building blocks. Keeping control of manufacture. *Crit. Rev. Biochem. Mol. Biol.* **47,** 50–63
4. Hu, C. M., and Chang, Z. F. (2007) Mitotic control of dTTP pool. A necessity or coincidence? *J. Biomed. Sci.* **14,** 491–497
5. Xu, X., Page, J. L., Surtees, J. A., Liu, H., Lagedrost, S., Lu, Y., Bronson, R., Alani, E., Nikitin, A. Y., and Weiss, R. S. (2008) Broad overexpression of ribonucleotide reductase genes in mice specifically induces lung neoplasms. *Cancer Res.* **68,** 2652–2660
6. Kolberg, M., Strand, K. R., Graff, P., and Andersson, K. K. (2004) Structure, function, and mechanism of ribonucleotide reductases. *Biochim. Biophys. Acta* **1699,** 1–34
7. Cotruvo, J. A., and Stubbe, J. (2011) Class I ribonucleotide reductases. Metallocofactor assembly and repair *in vitro* and *in vivo*. *Annu. Rev. Biochem.* **80,** 733–767
8. Kashlan, O. B., and Cooperman, B. S. (2003) Comprehensive model for allosteric regulation of mammalian ribonucleotide reductase. Refinements and consequences. *Biochemistry* **42,** 1696–1706
9. Stubbe, J., Nocera, D. G., Yee, C. S., and Chang, M. C. (2003) Radical initiation in the class I ribonucleotide reductase. Long-range proton-coupled electron transfer? *Chem. Rev.* **103,** 2167–2201
10. Thelander, L., and Reichard, P. (1979) Reduction of ribonucleotides. *Annu. Rev. Biochem.* **48,** 133–158
11. Ekberg, M., Sahlin, M., Eriksson, M., and Sjöberg, B. M. (1996) Two conserved tyrosine residues in protein R1 participate in an intermolecular electron transfer in ribonucleotide reductase. *J. Biol. Chem.* **271,** 20655–20659
12. Ando, N., Brignole, E. J., Zimanyi, C. M., Funk, M. A., Yokoyama, K., Asturias, F. J., Stubbe, J., and Drennan, C. L. (2011) Structural interconversions modulate activity of *Escherichia coli* ribonucleotide reductase. *Proc. Natl. Acad. Sci. U.S.A.* **108,** 21046–21051
13. von Döbeln, U., and Reichard, P. (1976) Binding of substrates to *Escherichia coli* ribonucleotide reductase. *J. Biol. Chem.* **251,** 3616–3622
14. Rofougaran, R., Crona, M., Vodnala, M., Sjöberg, B. M., and Hofer, A. (2008) Oligomerization status directs overall activity regulation of the *Escherichia coli* class Ia ribonucleotide reductase. *J. Biol. Chem.* **283,** 35310–35318
15. Huang, M., and Elledge, S. J. (1997) Identification of RNR4, encoding a second essential small subunit of ribonucleotide reductase in *Saccharomyces cerevisiae*. *Mol. Cell. Biol.* **17,** 6105–6113
16. Wang, P. J., Chabes, A., Casagrande, R., Tian, X. C., Thelander, L., and Huffaker, T. C. (1997) Rnr4p, a novel ribonucleotide reductase small-subunit protein. *Mol. Cell. Biol.* **17,** 6114–6121
17. Zhang, Y., An, X., Stubbe, J., and Huang, M. (2013) Investigation of *in vivo* roles of the carboxyl-terminal tails of the small subunit ($\beta\beta'$) of *S. cerevisiae* ribonucleotide reductase. Contribution to cofactor formation and inter-subunit association within the active holoenzyme. *J. Biol. Chem.* **288,** 13951–13959
18. Rofougaran, R., Vodnala, M., and Hofer, A. (2006) Enzymatically active mammalian ribonucleotide reductase exists primarily as an $\alpha_6\beta_2$ octamer. *J. Biol. Chem.* **281,** 27705–27711
19. Wang, J., Lohman, G. J., and Stubbe, J. (2007) Enhanced subunit interactions with gemcitabine-5′-diphosphate inhibit ribonucleotide reductases. *Proc. Natl. Acad. Sci. U.S.A.* **104,** 14324–14329
20. Fairman, J. W., Wijerathna, S. R., Ahmad, M. F., Xu, H., Nakano, R., Jha, S., Prendergast, J., Welin, R. M., Flodin, S., Roos, A., Nordlund, P., Li, Z., Walz, T., and Dealwis, C. G. (2011) Structural basis for allosteric regulation of human ribonucleotide reductase by nucleotide-induced oligomerization. *Nat. Struct. Mol. Biol.* **18,** 316–322
21. Scott, C. P., Kashlan, O. B., Lear, J. D., and Cooperman, B. S. (2001) A quantitative model for allosteric control of purine reduction by murine ribonucleotide reductase. *Biochemistry* **40,** 1651–1661
22. Eriksson, M., Uhlin, U., Ramaswamy, S., Ekberg, M., Regnström, K., Sjöberg, B. M., and Eklund, H. (1997) Binding of allosteric effectors to ribonucleotide reductase protein R1. Reduction of active-site cysteines promotes substrate binding. *Structure* **5,** 1077–1092
23. Thelander, M., Gräslund, A., and Thelander, L. (1985) Subunit M2 of mammalian ribonucleotide reductase. Characterization of a homogeneous protein isolated from M2-overproducing mouse cells. *J. Biol. Chem.* **260,** 2737–2741
24. Eklund, H., Uhlin, U., Färnegårdh, M., Logan, D. T., and Nordlund, P.

(2001) Structure and function of the radical enzyme ribonucleotide reductase. *Prog. Biophys. Mol. Biol.* **77,** 177–268
25. Sjöberg, B. M., Karlsson, M., and Jörnvall, H. (1987) Half-site reactivity of the tyrosyl radical of ribonucleotide reductase from *Escherichia coli*. *J. Biol. Chem.* **262,** 9736–9743
26. Massova, I., and Kollman, P. A. (1999) Computational alanine scanning to probe protein-protein interactions: A novel approach to evaluate binding free energies. *J. Am. Chem. Soc.* **121,** 8133–8143
27. Hou, T., Wang, J., Li, Y., and Wang, W. (2011) Assessing the performance of the MM/PBSA and MM/GBSA methods. 1. The accuracy of binding free energy calculations based on molecular dynamics simulations. *J. Chem. Inf. Model.* **51,** 69–82
28. Kollman, P. A., Massova, I., Reyes, C., Kuhn, B., Huo, S., Chong, L., Lee, M., Lee, T., Duan, Y., Wang, W., Donini, O., Cieplak, P., Srinivasan, J., Case, D. A., and Cheatham, T. E. (2000) Calculating structures and free energies of complex molecules. Combining molecular mechanics and continuum models. *Acc. Chem. Res.* **33,** 889–897
29. Case, D. A., Cheatham, T. E., 3rd, Darden, T., Gohlke, H., Luo, R., Merz, K. M., Jr., Onufriev, A., Simmerling, C., Wang, B., and Woods, R. J. (2005) The Amber biomolecular simulation programs. *J. Comput. Chem.* **26,** 1668–1688
30. Duan, Y., Wu, C., Chowdhury, S., Lee, M. C., Xiong, G., Zhang, W., Yang, R., Cieplak, P., Luo, R., Lee, T., Caldwell, J., Wang, J., and Kollman, P. (2003) A point-charge force field for molecular mechanics simulations of proteins based on condensed-phase quantum mechanical calculations. *J. Comput. Chem.* **24,** 1999–2012
31. Mark, P., and Nilsson, L. (2001) Structure and dynamics of the TIP3P, SPC, and SPC/E water models at 298 K. *J. Phys. Chem. A* **105,** 9954–9960
32. Ryckaert, J.-P., Ciccotti, G., and Berendsen, H. J. C. (1977) Numerical integration of the cartesian equations of motion of a system with constraints. Molecular dynamics of *n*-alkanes. *J. Comput. Phys.* **23,** 327–341
33. Darden, T., York, D., and Pedersen, L. (1993) Particle mesh Ewald. An N [center-dot] log(*N*) method for Ewald sums in large systems. *J. Chem. Phys.* **98,** 10089–10092
34. Essmann, U., Perera, L., Berkowitz, M. L., Darden, T., Lee, H., and Pedersen, L. G. (1995) A smooth particle mesh Ewald method. *J. Chem. Phys.* **103,** 8577–8593
35. Shao, J., Zhou, B., Zhu, L., Qiu, W., Yuan, Y. C., Xi, B., and Yen, Y. (2004) *In vitro* characterization of enzymatic properties and inhibition of the p53R2 subunit of human ribonucleotide reductase. *Cancer Res.* **64,** 1–6
36. Shao, J., Zhou, B., Zhu, L., Bilio, A. J., Su, L., Yuan, Y.-C., Ren, S., Lien, E. J., Shih, J., and Yen, Y. (2005) Determination of the potency and subunit-selectivity of ribonucleotide reductase inhibitors with a recombinant-holoenzyme-based *in vitro* assay. *Biochem. Pharmacol.* **69,** 627–634
37. Xue, L., Zhou, B., Liu, X., Qiu, W., Jin, Z., and Yen, Y. (2003) Wild-type p53 regulates human ribonucleotide reductase by protein-protein interaction with p53R2 as well as hRRM2 subunits. *Cancer Res.* **63,** 980–986
38. Zhu, L., Zhou, B., Chen, X., Jiang, H., Shao, J., and Yen, Y. (2009) Inhibitory mechanisms of heterocyclic carboxaldehyde thiosemicabazones for two forms of human ribonucleotide reductase. *Biochem. Pharmacol.* **78,** 1178–1185
39. Zhou, B. S., Ker, R., Ho, R., Yu, J., Zhao, Y. R., Shih, J., and Yen, Y. (1998) Determination of deoxyribonucleoside triphosphate pool sizes in ribonucleotide reductase cDNA transfected human KB cells. *Biochem. Pharmacol.* **55,** 1657–1665
40. Thelander, L., Gräslund, A., and Thelander, M. (1983) Continual presence of oxygen and iron required for mammalian ribonucleotide reduction. Possible regulation mechanism. *Biochem. Biophys. Res. Commun.* **110,** 859–865
41. Tarpey, M. M., Wink, D. A., and Grisham, M. B. (2004) Methods for detection of reactive metabolites of oxygen and nitrogen. *In vitro* and *in vivo* considerations. *Am. J. Physiol. Regul. Integr. Comp. Physiol.* **286,** R431–R444
42. Qi, H., Zhu, H., Lou, M., Fan, Y., Liu, H., Shen, J., Li, Z., Lv, X., Shan, J., Zhu, L., Chin, Y. E., and Shao, J. (2012) Interferon regulatory factor 1 transactivates expression of human DNA polymerase η in response to carcinogen *N*-methyl-*N*′-nitro-*N*-nitrosoguanidine. *J. Biol. Chem.* **287,** 12622–12633
43. Narváez, A. J., Voevodskaya, N., Thelander, L., and Gräslund, A. (2006) The involvement of Arg^{265} of mouse ribonucleotide reductase R2 protein in proton transfer and catalysis. *J. Biol. Chem.* **281,** 26022–26028
44. Liu, X., Zhou, B., Xue, L., Shih, J., Tye, K., Qi, C., and Yen, Y. (2005) The ribonucleotide reductase subunit M2B subcellular localization and functional importance for DNA replication in physiological growth of KB cells. *Biochem. Pharmacol.* **70,** 1288–1297
45. Nordlund, P., and Eklund, H. (1993) Structure and function of the Escherichia coli ribonucleotide reductase protein R2. *J. Mol. Biol.* **232,** 123–164
46. Chabes, A., Domkin, V., Larsson, G., Liu, A., Graslund, A., Wijmenga, S., and Thelander, L. (2000) Yeast ribonucleotide reductase has a heterodimeric iron-radical-containing subunit. *Proc. Natl. Acad. Sci. U.S.A.* **97,** 2474–2479
47. Strand, K. R., Karlsen, S., and Andersson, K. K. (2002) Cobalt substitution of mouse R2 ribonucleotide reductase as a model for the reactive diferrous state. Spectroscopic and structural evidence for a ferromagnetically coupled dinuclear cobalt cluster. *J. Biol. Chem.* **277,** 34229–34238
48. Kauppi, B., Nielsen, B. B., Ramaswamy, S., Larsen, I. K., Thelander, M., Thelander, L., and Eklund, H. (1996) The three-dimensional structure of mammalian ribonucleotide reductase protein R2 reveals a more-accessible iron-radical site than *Escherichia coli* R2. *J. Mol. Biol.* **262,** 706–720
49. Strand, K. R., Karlsen, S., Kolberg, M., Røhr, A. K., Görbitz, C. H., and Andersson, K. K. (2004) Crystal structural studies of changes in the native dinuclear iron center of ribonucleotide reductase protein R2 from mouse. *J. Biol. Chem.* **279,** 46794–46801
50. Chabes, A. L., Pfleger, C. M., Kirschner, M. W., and Thelander, L. (2003) Mouse ribonucleotide reductase R2 protein: a new target for anaphase-promoting complex-Cdh1-mediated proteolysis. *Proc. Natl. Acad. Sci. U.S.A.* **100,** 3925–3929
51. Chabes, A. L., Björklund, S., and Thelander, L. (2004) S phase-specific transcription of the mouse ribonucleotide reductase R2 gene requires both a proximal repressive E2F-binding site and an upstream promoter activating region. *J. Biol. Chem.* **279,** 10796–10807
52. Tanaka, H., Arakawa, H., Yamaguchi, T., Shiraishi, K., Fukuda, S., Matsui, K., Takei, Y., and Nakamura, Y. (2000) A ribonucleotide reductase gene involved in a p53-dependent cell-cycle checkpoint for DNA damage. *Nature* **404,** 42–49
53. Engström, Y., Rozell, B., Hansson, H. A., Stemme, S., and Thelander, L. (1984) Localization of ribonucleotide reductase in mammalian cells. *EMBO J.* **3,** 863–867
54. Reddy, G. P., and Fager, R. S. (1993) Replitase. A complex integrating dNTP synthesis and DNA replication. *Crit. Rev. Eukaryot. Gene Expr.* **3,** 255–277
55. Lee, Y. D., and Elledge, S. J. (2006) Control of ribonucleotide reductase localization through an anchoring mechanism involving Wtm1. *Genes Dev.* **20,** 334–344
56. Wu, X., and Huang, M. (2008) Dif1 controls subcellular localization of ribonucleotide reductase by mediating nuclear import of the R2 subunit. *Mol. Cell. Biol.* **28,** 7156–7167
57. Nocentini, G. (1996) Ribonucleotide reductase inhibitors. New strategies for cancer chemotherapy. *Crit. Rev. Oncol. Hematol.* **22,** 89–126
58. Shao, J., Zhou, B., Chu, B., and Yen, Y. (2006) Ribonucleotide reductase inhibitors and future drug design. *Curr. Cancer Drug Targets* **6,** 409–431

The Conserved Lys-95 Charged Residue Cluster Is Critical for the Homodimerization and Enzyme Activity of Human Ribonucleotide Reductase Small Subunit M2

Xinhuan Chen, Zhijian Xu, Lingna Zhang, Hongchuan Liu, Xia Liu, Meng Lou, Lijun Zhu, Bingding Huang, Cai-Guang Yang, Weiliang Zhu and Jimin Shao

J. Biol. Chem. 2014, 289:909-920.
doi: 10.1074/jbc.M113.524546 originally published online November 19, 2013
